scientific reports

Check for updates

OPEN

Sodium butyrate attenuates sodium fluoride-induced cardiac injury in rats via modulating oxidative stress, inflammation, and apoptosis

Lu Meng[1,2,3,10], Nan Yan[4,8,10], Xin Li[2,3,5,9], Zhenxiang Sun[1,2,3], Mengru Qin[1,2,3], Shuyu Liu[1,2,3], Xiaoxu Duan[6], Yubo Zhao[1,2,3], Zhe Zhang[1,2,3], Qianyu Li[1,2,3], Bing Shao[7], Fu Ren[1,2,3]✉ & Zhengdong Wang[1,2,3]✉

As a well-recognized double-edged element in health and disease, low concentrations of fluoride are beneficial for preventing dental caries, but chronic exposure to excessive fluoride induces multi-system toxicity, including cardiotoxicity, for which no specific therapeutic agents are currently available. This study explored whether sodium butyrate (NaB), a natural derivative of short-chain fatty acids, attenuates sodium fluoride (NaF)-induced cardiac injury in rats by regulating oxidative stress, inflammation, and apoptosis. Forty-eight Sprague-Dawley rats were randomized into Control, NaB, NaF, and NaF + NaB groups. After 17 weeks of NaF exposure (NaB co-administered in the last 4 weeks), cardiac injury was assessed via histopathology, myocardial biomarkers, and molecular assays for oxidative stress, inflammation, and apoptosis. NaF exposure reduced the heart-to-brain weight ratio by 17.8%, dysregulated biomarkers (cTnI ↓19.3%, LDH ↑20.5%), induced histopathological damage, and disrupted oxidative stress (MDA ↑21.5%, SOD ↓19.2%, CAT ↓26.1%), inflammation (TNF-α ↑40.1%, IL-6 ↑27.9%, IL-10 ↓21.9%), and apoptosis (cleaved Caspase-3/pro-Caspase-3 ratio ↑51.1%, Bcl-2/Bax ratio ↓53.5%). NaB reversed these changes, restoring myocardial structure and molecular homeostasis. These findings indicate that NaB alleviates NaF-induced cardiac injury through antioxidant, anti-inflammatory, and anti-apoptotic effects, suggesting it may serve as a potential natural therapeutic agent for fluoride-associated cardiac injury.

Keywords Fluoride toxicity, Sodium butyrate, Cardiotoxicity, Oxidative stress, Inflammation, Apoptosis

Fluoride (F) is a common environmental pollutant entering ecosystems through geological leaching, industrial emissions, and agricultural runoff[1]. Chronic exposure to elevated fluoride levels (>1.5 mg/L) affects over 200 million people worldwide, inducing multisystem toxicity including cardiotoxicity[2–4]. Notably, epidemiological studies report a significant correlation between high fluoride intake and increased prevalence of cardiovascular diseases in endemic fluorosis areas[5], and fluoride exposure can induce cardiotoxicity, leading to cardiac injury (structural and functional alterations)[6,7]. A cross-sectional study in China's fluorosis endemic areas found that adults with high fluoride exposure had a significantly increased risk of hypertension and cardiac dysfunction (Xiang et al., 2020). In addition, a study in 2025 found that environmental fluoride exposure

[1]Department of Human Anatomy, School of Basic Medicine, Shenyang Medical College, Shenyang, P. R. China. [2]Liaoning Province Key Laboratory for Phenomics of Human Ethnic Specificity and Critical Illness, Shenyang Medical College, Shenyang, P. R. China. [3]Shenyang Key Laboratory for Phenomics, Shenyang Medical College, Shenyang, P. R. China. [4]School of Shuren International, Shenyang Medical College, Shenyang, P. R. China. [5]School of Stomatology, Shenyang Medical College, Shenyang, P. R. China. [6]School of Public Health, Shenyang Medical College, Shenyang, P. R. China. [7]Department of Cardiology, Second Hospital of Shenyang Medical College, Shenyang, P. R. China. [8]School of Innovation and Entrepreneurship, Shenyang Medical College, Shenyang, P. R. China. [9]Shenyang Key Laboratory of Prevention and Treatment of Systemic Important Diseases, Shenyang Medical College, Shenyang, P. R. China. [10]Lu Meng and Nan Yan contributed equally to this work. ✉email: rf@symc.edu.cn; wangzhengdong@symc.edu.cn

(> 2 mg/L in drinking water) was associated with subclinical cardiac structural changes[8], including decreased left ventricular mass index, in childre—highlighting that fluoride cardiotoxicity spans all age groups and represents a long-term global health burden with no approved interventions.

The mechanisms underlying fluoride-induced cardiac injury are complex and involve oxidative stress, inflammation, and apoptosis[9,10]. Oxidative stress, characterized by an imbalance between reactive oxygen species (ROS) generation and antioxidant defense, can induce lipid peroxidation, protein modification, and DNA damage, ultimately compromising cellular function[11,12]. The inflammatory response triggered by fluoride exposure promotes the release of pro-inflammatory cytokines (e.g., IL-6, TNF-α), exacerbating tissue damage[13]. Furthermore, dysregulation of apoptosis, a programmed cell death process, leads to cardiomyocyte loss, consequently contributing to cardiac dysfunction[14,15]. Despite the established cardiotoxicity of fluoride, effective therapeutic strategies are still limited[16,17].Notably, chronic fluoride-induced cardiac injury also involves electrolytic imbalance (e.g., hyponatremia/hyperkalemia causing bradycardia), calcium dysregulation, and ATP depletion, which synergize with the oxidative stress-inflammation-apoptosis axis[9,18]. For instance, fluoride-induced ROS overproduction can directly trigger calcium overload, while apoptotic mitochondrial damage further reduces ATP synthesis[19].

Sodium butyrate (NaB) is a gut microbiota-derived short-chain fatty acid with low toxicity and cost—advantages for drug development and functional additives. Critically, it has demonstrated therapeutic potential in various diseases owing to its antioxidant[20], anti-inflammatory[21], and anti-apoptotic properties[22]. For instance, in liver injury models, NaB has been shown to enhance antioxidant enzyme activity[23], reduce lipid peroxidation, exert anti-inflammatory effects by inhibiting NLRP3 inflammasome activation[24], and ameliorate fluoride-induced apoptosis via the mitophagy pathway[25]. In neurodegenerative disease models, NaB inhibits neuroinflammation by downregulating pro-inflammatory cytokines and reduces fluoride induced neurotoxicity by regulating hippocampal glycolysis[26,27]. Notably, NaB ameliorates cardiac injury in metabolic and ischemic models by restoring redox balance and inhibiting cardiomyocyte death[28]. However, a critical gap remains: despite NaB's broad cytoprotective effects, its efficacy against cardiotoxicity induced by chronic environmental pollutants—particularly fluoride—has never been investigated. Previous studies on NaB and cardiac health focus on metabolic or ischemic damage, not toxicant-driven pathology; similarly, research on fluoride cardiotoxicity lacks exploration of natural therapeutic agents. This gap leaves no evidence-based options for protecting populations in fluorosis endemic areas from cardiac injury.

Therefore, this study aimed to investigate the protective effects of NaB against NaF-induced cardiac injury in rats and to explore the underlying mechanisms involving oxidative stress, inflammation, and apoptosis.

Based on the above gaps, we hypothesized that NaB alleviates NaF-induced cardiac injury in rats by modulating the oxidative stress-inflammation-apoptosis axis. To test this hypothesis, the study had three specific aims: (1) Validate the NaF-induced cardiac injury model via serum/urinary fluoride detection, cardiac morphometric analysis (heart-to-brain weight ratio), and histopathological assessment; (2) Evaluate NaB's protective effects on NaF-induced cardiac damage by quantifying myocardial biomarkers (cTnI, LDH) and restoring tissue structure; (3) Uncover the underlying mechanism by measuring oxidative stress markers (MDA, SOD, CAT), inflammatory cytokines (TNF-α, IL-6, IL-10), and apoptosis regulators (Bcl-2, Bax, Caspase-3) in cardiac tissue.

Materials and methods

Chemical reagents

(Sodium fluoride) NaF and Sodium butyrate (NaB) were purchased from MACKLIN Biological Reagent (Shanghai, China). BCA, RIPA, and PMSF reagents were obtained from Beijing Dingguo Changsheng Biotechnology (Shenyang, China). ELISA kits for myocardial injury biomarkers (cardiac troponin I [cTnI] and lactate dehydrogenase [LDH]), oxidative stress marker superoxide dismutase [SOD], and inflammatory cytokines (tumor necrosis factor-α [TNF-α], interleukin-6 [IL-6], and interleukin-10 [IL-10]) were sourced from Byabscience Biotechnology Co., Ltd (Nanjing, China). Kits for MDA and CAT were provided by Nanjing Jiancheng (Nanjing, China). Antibodies for Western blot analysis were procured from HuaBio (Hangzhou, China) and Proteintech Group, Inc (Wuhan, China).

Experimental animals

Forty-eight male Sprague-Dawley (SD) rats (4 weeks old, 250–280 g) were obtained from Beijing HFK Biotechnology (Beijing, China) and were part of the same cohort used in a previous study[25]. Rats were housed in polypropylene cages (4 rats per cage, 45 × 30 × 20 cm) under standard conditions (12-h light/dark cycle, 24 ± 1 °C, 45 ± 5% humidity) with ad libitum access to food and water. Environmental enrichment was provided, including wooden chew sticks and plastic nesting materials, to minimize stress. All animal experimental methods were performed in accordance with the relevant guidelines and regulations, including the ARRIVE 2.0 guidelines and the ethical standards approved by the Animal Ethics Committee of Shenyang Medical College (SYYXY2023051001).

Experimental design

The animal model used in this study was the same as that described in our previously published work by[25]. Rats ($n = 48$) were stratified by body weight and randomly assigned to four groups ($n = 12$) using a computer-generated sequence by an independent statistician, with allocation concealed in opaque envelopes. The groups were as follows: (1) Control: distilled water + saline gavage; (2) NaF: 100 mg/L NaF water + saline gavage; (3) NaB: distilled water + 1000 mg/kg NaB gavage; (4) NaF + NaB: 100 mg/L NaF water + 1000 mg/kg NaB gavage.

Blinding was maintained for personnel involved in daily administration and all endpoint analyses throughout the study. Fluoride exposure and NaB administration protocols were performed according to[25], with NaB delivered by gavage to ensure precise dosing and bioavailability.

After 17 weeks, rats were euthanized via sodium pentobarbital injection (200 mg/kg, i.p.). Blood collected from the abdominal aorta was centrifuged (3,000 rpm, 10 min) for serum fluoride analysis. Urine was obtained via 24-h metabolic cage collection. Three rats per group underwent transcardial perfusion with 4% paraformaldehyde for histopathology; remaining hearts were stored at -80 °C for molecular assays.

Assessment of dental fluorosis

Dental fluorosis was evaluated according to a modified Dean's index. All rats were examined under standardized lighting conditions by two independent investigators blinded to the experimental groups. The lower incisors were visually inspected for enamel changes such as opacities, discolorations, and surface integrity. Each tooth was assigned a score from 0 (normal) to 3 (moderate/severe fluorosis), corresponding to the established categories of the index. For statistical analysis, teeth with a Dean' s score ≥ 1 were considered positive for dental fluorosis. The inter-examiner reliability was confirmed by Cohen's kappa coefficient (> 0.85).

Fluoride ion detection

Fluoride concentrations in serum and urine were measured using a validated fluoride ion-selective electrode method[25]. Briefly, samples were diluted 1:1 with TISAB buffer (Thunder Magnetic Instruments, Shanghai, China), and concentrations were read using a fluoride ion meter calibrated with fluoride standards (Thunder Magnetic Instruments, Shanghai, China).

Measurement of cardiac injury markers

Cardiac tissue (10 mg) was homogenized in 100 μL PBS. Levels of cardiac troponin I (cTnI) and lactate dehydrogenase (LDH) were quantified using ELISA kits (Byabscience Biotechnology Co., Ltd) according to the manufacturer's instructions. Standards (50 μL) were added to standard wells, samples (50 μL) to sample wells, and 100 μL HRP-conjugated antibody to all wells except blanks. After incubation (37 °C, 60 min), plates were washed five times. Substrate solution (100 μL, 1:1 mixture of substrates A and B) was added, incubated (37 °C, 15 min), and reactions stopped with 50 μL stop solution. Absorbance was read at 450 nm.

Measurement of antioxidant and oxidative stress parameters

Cardiac tissue was homogenized in deionized water (1:9 w/v). Supernatants were collected after centrifugation (12,000 rpm, 15 min). MDA levels and CAT activity were measured using kits (Nanjing Jiancheng). T-SOD levels determined by ELISA (Byabscience Biotechnology Co., Ltd). Protein concentrations were assayed using a BCA kit (Beijing Dingguo Changsheng Biotechnology).

Measurement of inflammatory cytokines

Cardiac tissue (10 mg) was homogenized in 100 μL PBS. Levels of TNF-α, IL-6, and IL-10 were quantified using ELISA kits (Byabscience Biotechnology Co., Ltd, Nanjing) as described in Sect. 2.6.

Western blot analysis

Cardiac tissue total proteins were extracted utilizing RIPA buffer (Beijing Dingguo Changsheng Biotechnology, Shenyang) mixed with PMSF at a 100:1 volume ratio. The BCA assay was applied to determine protein concentrations. A 27 μg aliquot of each protein sample was loaded onto 12.5% SDS-PAGE gels for separation, followed by transfer onto PVDF membranes (Merck Millipore, USA). After blocking with 5% skim milk for 2 h at room temperature, membranes were probed overnight at 4 °C with the following primary antibodies: Bcl-2 (1:2000; HuaBio), Bax (1:8000; Proteintech Group, Inc), Caspase-3 (1:500; Proteintech Group, Inc), and GAPDH (1:10,000; Proteintech Group, Inc). Following TBST washes, membranes were incubated with HRP-conjugated secondary antibody (1:8000; Beijing Dingguo Changsheng Biotechnology) for 2 h at room temperature. Chemiluminescent signals were developed using ECL reagent (Biyuntian, Dalian, China) and captured with a ChemiDoc system (Bio-Rad, USA). Band densitometry was analyzed using ImageJ 1.4 software (NIH, USA).

Gene expression analysis

Total RNA was extracted using a kit (Magen, Guangzhou), and cDNA was synthesized with a reverse transcription kit (Takara, Dalian). Real-Time Quantitative Reverse Transcription Polymerase Chain Reaction(RT-qPCR) was performed on a Bio-Rad CFX96 system using primers listed in Table 1. RPL13A was used as the housekeeping gene for normalization. Relative gene expression was calculated via the $2^{-\Delta\Delta Ct}$ method.

Histopathological analysis

Tissue samples were fixed in 4% paraformaldehyde for 24–48 h, dehydrated through a graded ethanol series (70%, 80%, 90%, 95%, and 100%), cleared in xylene, and embedded in paraffin. Sections (4–5 μm thick) were cut using a microtome (Leica RM2235, Germany), mounted on glass slides, and dried at 60 °C for 2 h, and then stained with hematoxylin and eosin (H&E). Images were acquired using an optical microscope (Motic, Xiamen, China).

TUNEL assay for apoptosis

Cardiac apoptosis was evaluated by TUNEL staining (TUNEL Cell Apoptosis Detection Kit, Doctoral Bioengineering) following the manufacturer's protocol. In brief, deparaffinized cardiac tissue sections were treated with proteinase K (20 μg/mL, 20 min) and incubated with the TUNEL reaction mix (37 °C, 1 h). Apoptotic nuclei were visualized with HRP-conjugated DAB, counterstained with hematoxylin, and imaged under a light microscope (Motic) at 40× magnification.

Gene symbol	Primer direction	Sequence (5' → 3')	Product size (bp)
Tnf	Forward	ATGTGGAACTGGCAGAGGAG	127
Tnf	Reverse	AGTAGACAGAAGAGCGTGGTG	127
Il6	Forward	TCCTACCCCAACTTCCAATGC	139
Il6	Reverse	GGTTTGCCGAGTAGACCTCAT	139
Il10	Forward	TTGAACCACCCGGCATCTAC	116
Il10	Reverse	TGGAGAGAGGTACAAACGAGG	116
Bax	Forward	GCAGACGGCAACTTCAACT	259
Bax	Reverse	TGGTGAGTGAGGCAGTGAG	259
Bcl2	Forward	GTGTGGAGAGCGTCAACAG	182
Bcl2	Reverse	CTTCAGAGACAGCCAGGAGA	182
Casp3	Forward	GGAGCTTGGAACGCGAAGA	169
Casp3	Reverse	ACACAAGCCCATTTCAGGGT	169
Rpl13a	Forward	CGCCTCAAGGTGTTGGATG	161
Rpl13a	Reverse	GCTGTCACTGCCTGGTACT	161

Table 1. Primer base sequence of RT-qPCR detection.

The apoptotic index, defined as the percentage of TUNEL-positive (brown) nuclear area relative to the total tissue area, was quantified using ImageJ 1.4 software. For each group ($n = 3$ rats), three non-overlapping fields from the left ventricular free wall per section were analyzed. The final index per group represents the mean value derived from nine fields (3 fields/rat × 3 rats/group).

Organ coefficient
Heart-to-brain weight ratio = [Absolute Heart weight (g) / Absolute Brain weight (g)] × 100%.

Calculation of % change for key biomarkers (vs. control group)
% Change = [(NaF Group Mean - Control Group Mean) / Control Group Mean] × 100%.

Statistical analysis
Sample sizes were determined a priori using G*Power 3.1. For in vivo studies, a sample size of 12 rats per group was chosen to detect a 20% difference in the primary endpoint (heart-to-brain weight ratio) with $\alpha = 0.05$ and 80% power, accounting for potential attrition (which did not occur). For in vitro assays, 3–6 replicates per group were used, as established in standard protocols. Data are presented as mean ± SD. All statistical analyses were performed using GraphPad Prism 8. After confirming normality with the Shapiro-Wilk test, multiple comparisons were analyzed by one-way ANOVA followed by Tukey's post-hoc test. Experiments were independently repeated at least three times. Statistical significance was defined as $^{*}p < 0.05$, $^{**}p < 0.01$, $^{***}p < 0.001$, and $^{****}p < 0.0001$.

Results
Model validation & NaB efficacy
As established in our previous model[25], the NaF group exhibited a 100% incidence of dental fluorosis (Dean score ≥ 1) alongside significantly elevated systemic fluoride, with serum and urinary levels 41% (0.1565 vs. 0.1110 mg/L; $p < 0.001$) and 375% (8.139 vs. 1.715 mg/L; $p < 0.0001$) higher than Controls, respectively. NaF + NaB co-treatment effectively mitigated this burden, reducing fluorosis incidence to 90% and significantly lowering both serum and urinary fluoride. Consistent with the clinical severity observed by Dean's index, this gradient of fluoride accumulation (NaF > NaF + NaB > Control/NaB) aligned with cardiac injury biomarker levels: LDH followed the same trend, while cTnI showed an inverse pattern. Throughout the 17-week study, no mortality occurred. The NaF group displayed marked lethargy, reduced intake, and rough fur, which were partially ameliorated by NaB administration after two weeks.

Cardiac morphometric parameters
Compared to controls, NaF exposure reducing both heart weight and brain weight. However, heart to brain weight ratio significantly decreased ($p < 0.01$), indicating that the heart is the main target organ (degree of damage > brain) (Table 2).

NaB treatment normalizes the ratio of heart to brain weight ratio, with no significant effect on brain weight ($p > 0.05$). This demonstrates NaB targeted cardioprotection against NaF induced toxicity. (Table 2).

Cardiac injury assessment
NaF exposure induced significant cardiac injury, as evidenced by both biomarker dysregulation and histopathological alterations. At the molecular level, NaF exposure caused paradoxical biomarker changes: cTnI decreased significantly vs. controls ($p < 0.001$, indicating myofibrillar degradation/atrophy), while LDH increased ($p < 0.001$, reflecting membrane damage). Sodium butyrate treatment effectively ameliorated both alterations (Fig. 1A, B). NaB alone had no adverse effects.

Group	Absolute heart weight (g)	Absolute brain weight(g)	Heart-to-brain weight ratio
Control	1.09 ± 0.05	2.07 ± 0.03	0.55 ± 0.01
NaB	1.10 ± 0.06	2.05 ± 0.03	0.55 ± 0.01
NaF	0.85 ± 0.04**	1.89 ± 0.03**	0.45 ± 0.02**
NaF + NaB	1.14 ± 0.02##	1.94 ± 0.04ns	0.54 ± 0.03#

Table 2. NaF and NaB effects on cardiac morphometric parameters. Note: Data are expressed as mean ± SEM ($n = 6$). **$p < 0.01$ vs. Control; #$p < 0.05$, ##$p < 0.01$, ns$p > 0.05$ vs. NaF (one-way ANOVA, GraphPad Prism 8).

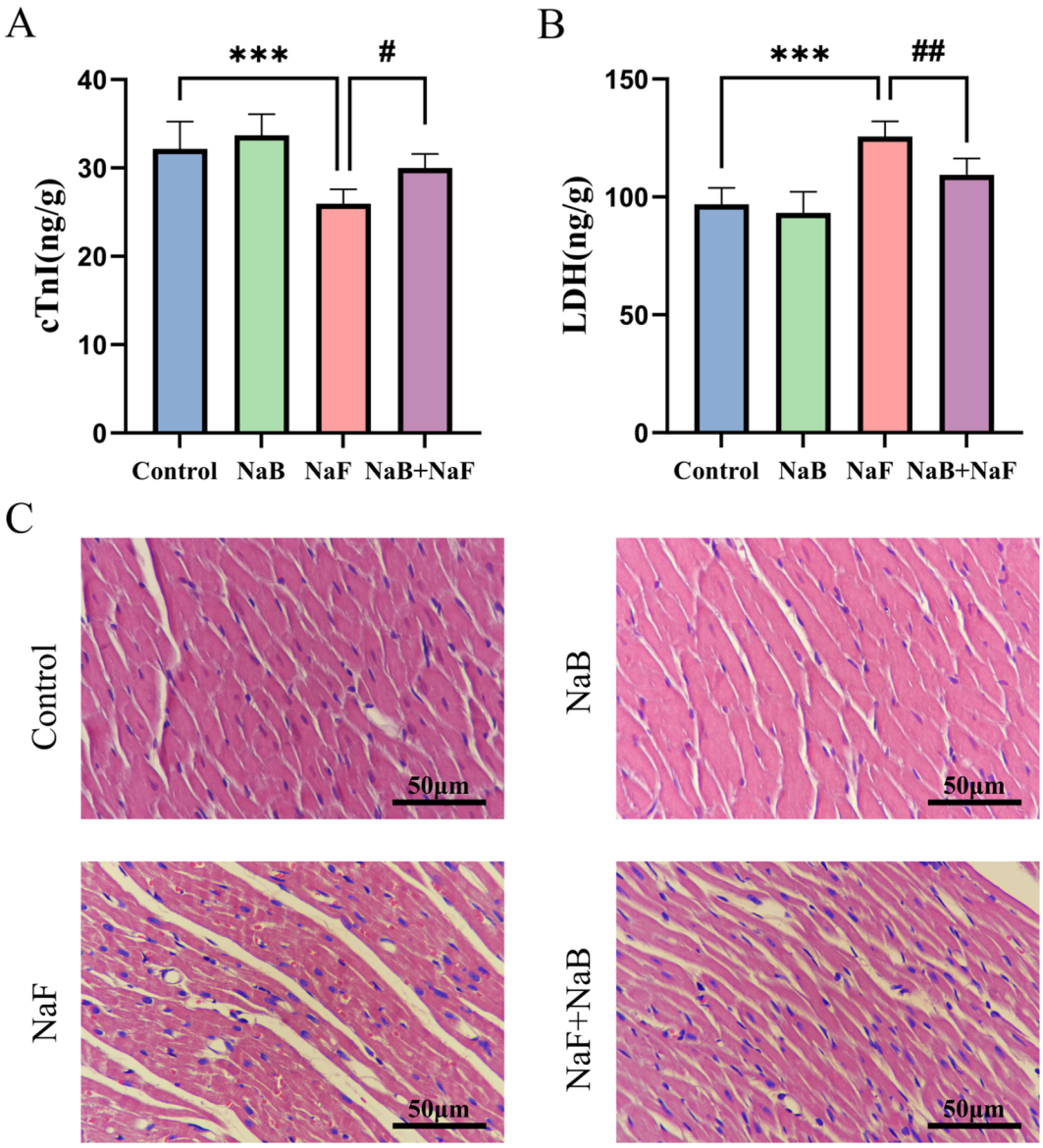

Fig. 1. NaF and NaB effects on myocardial injury biomarkers and cardiac histopathology. (A) cardiac troponin I (cTnI) levels in myocardial tissue homogenates; (B) lactate dehydrogenase (LDH) levels in myocardial tissue homogenates. Data are expressed as mean ± SEM ($n = 6$). ***$p < 0.001$ vs. Control; #$p < 0.05$, ##$p < 0.01$ vs. NaF (one-way ANOVA, GraphPad Prism 8); (C) Representative hematoxylin and eosin (H&E)-stained sections. Scale bar: 50 μm (40× objective lens).

H&E staining revealed severe histopathological alterations in NaF-exposed hearts: marked atrophy of cardiomyocytes, disorganized cellular arrangement, widened intercellular spaces, and prominent vacuolar degeneration (clear cytoplasmic vacuoles in a substantial subset of cardiomyocytes). These changes were consistently observed across all 3 tissue Sect. (1 section per rat, $n = 3$ rats per group). (Fig. 1C). In contrast,

NaF + NaB co-treatment attenuated these changes, showing restored cardiomyocyte morphology and reduced vacuolization. Control and NaB-alone groups displayed normal histology.

These qualitative observations are corroborated by quantitative myocardial biomarker data (↓cTnI by 19.3%, ↑LDH by 20.5% in the NaF group, both restored by NaB), confirming NaF-induced structural damage and NaB's protective effect.

Oxidative stress

Detecting the levels of lipid peroxide MDA, antioxidant enzyme SOD, and antioxidant enzyme CAT activity, and explore the effect of NaB on NaF induced oxidative stress state. As shown in Fig. 2, NaF exposure increased MDA levels and decreased SOD levels and CAT activity. NaB intervention effectively reversed these changes ($p < 0.05$). Indicating that NaB can alleviate NaF induced myocardial injury by inhibiting oxidative stress.

Inflammation

RT-qPCR was used to detect the mRNA levels of inflammatory factors *Tnf*, *Il6*, and *Il10* (Fig. 3A-C). The protein levels and mRNA expression trends of TNF - α, IL-6, and IL-10 detected by the ELISA kit were almost consistent (Fig. 3D-F). Exposure to NaF increases the levels of pro-inflammatory cytokines (TNF - α, IL-6) and inhibits anti-inflammatory IL-10 at both mRNA and protein levels. NaB treatment normalized these changes, reduced TNF - α/IL-6, and increased IL-10. This indicates that NaB intervention can reduce NaF induced inflammatory imbalance.

Apoptosis assessment (TUNEL)

To observe the regulatory effect of NaB on NaF induced cell apoptosis, TUNEL staining was performed on rat myocardial tissue; The results are shown in (Fig. 4A and B). TUNEL staining showed a significant increase in apoptosis of cardiac cells exposed to NaF compared to the control group; Compared with the NaF group, the NaF + NaB group reduced the degree of cell apoptosis. These results indicate that NaB improves cell apoptosis induced by NaF exposure.

Apoptosis regulators

To further demonstrate the regulatory effect of NaB on NaF induced cardiomyocyte apoptosis, we used RT qPCR and Western blot to evaluate the mRNA and protein levels of apoptosis regulatory factors Bax, Bcl2, and Caspase3, respectively. At mRNA level, NaF upregulated pro-apoptotic *Bax* and *Casp3* and downregulated anti-apoptotic *Bcl2* (Fig. 5A–C). Western blot analysis of key apoptosis regulators revealed that, compared to controls, NaF-exposed hearts exhibited: A significantly increased cleaved Caspase-3/pro-Caspase-3 ratio, indicating caspase activation; A markedly diminished Bcl-2/Bax ratio, reflecting pro-apoptotic shift. These protein-level changes (Fig. 5D–G) were consistent with the mRNA expression patterns (Fig. 5A–C). Critically, NaB intervention nearly normalized both ratios in the NaF + NaB group, collectively demonstrating its anti-apoptotic efficacy.

Discussion

Fluoride is an important toxicological and environmental toxin. A small intake of fluoride (< 0.5 mg/L) is beneficial for promoting dental health by reducing tooth decay, while exceeding the WHO limit of 1.5 mg/L may lead to fluorosis[29]. Global groundwater fluoride pollution has been documented in over 100 countries during the past decade, affecting > 200 million people worldwide through associated health complications[30]. Chronic fluoride exposure not only causes damage to the skeletal system[31], but also poses a significant threat to non-skeletal systems, such as inducing neurotoxicity[32] and cardiac dysfunction[33]. Therefore, the cardiac injury caused by chronic fluorosis is an urgent issue that needs to be addressed for populations in endemic fluorosis areas.

Fluoride's toxicity extends beyond the heart: it induces hepatic oxidative stress[24], renal inflammation[13], and neurotoxicity[27], all via the oxidative stress-inflammation-apoptosis axis mirrored in our cardiac findings.

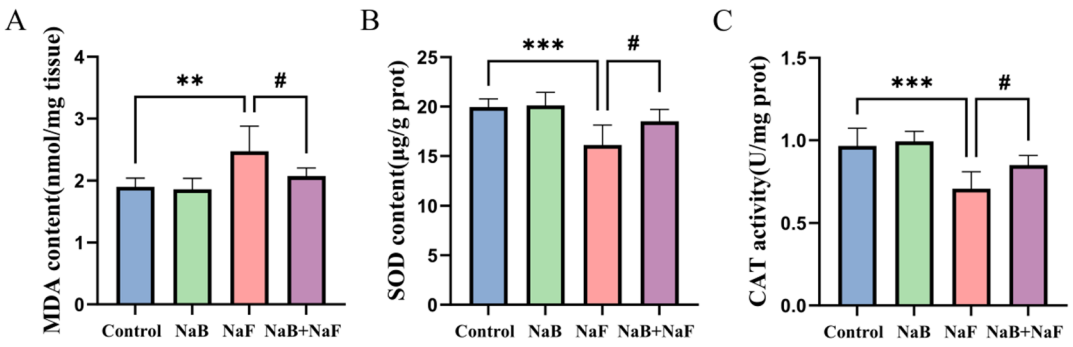

Fig. 2. NaF and NaB effects on oxidative stress biomarkers in cardiac tissue. (**A**) Measurement of malondialdehyde (MDA) levels in myocardial tissue of rats; (**B**) Measurement of superoxide dismutase (SOD) levels in myocardial tissue of rats; (**C**) Measurement of catalase (CAT) activity in myocardial tissue of rats. Data are expressed as mean ± SEM ($n = 6$). $^{**}p < 0.01$, $^{***}p < 0.001$ vs. Control; $^{\#}p < 0.05$ vs. NaF (one-way ANOVA, GraphPad Prism 8).

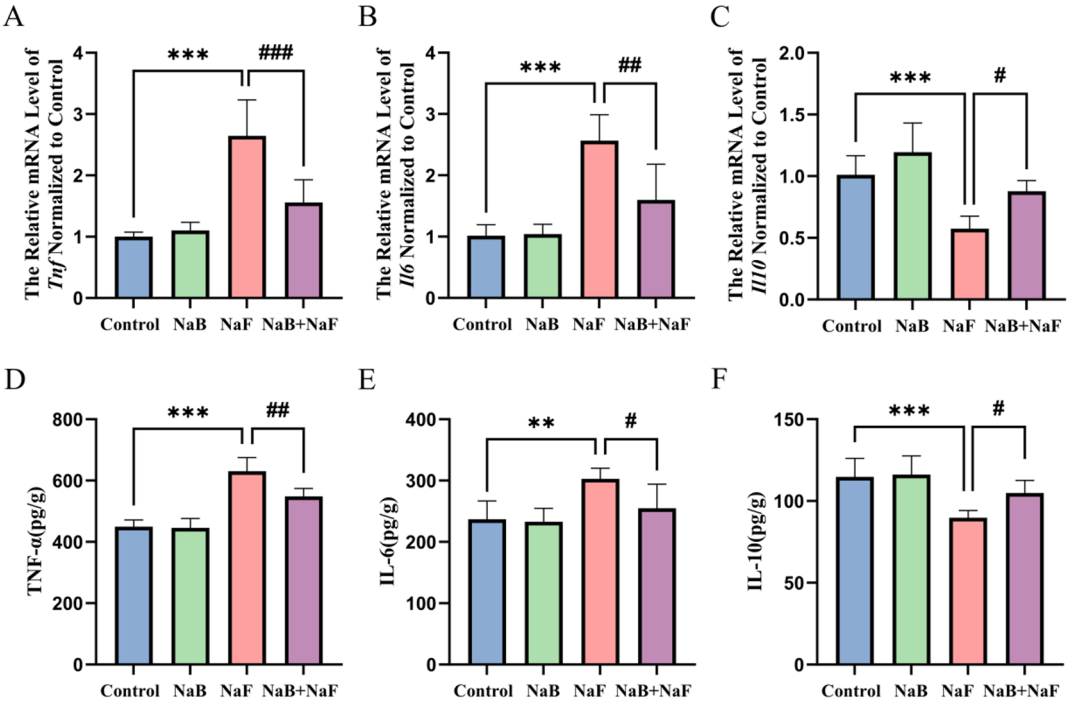

Fig. 3. NaF and NaB effects on inflammatory cytokines. RT-qPCR (mRNA) and ELISA (protein) were used to detect inflammatory cytokine expression. (**A**–**C**) mRNA levels of Tnf (tumor necrosis factor-α), Il6 (interleukin-6), Il10 (interleukin-10); (**D**–**F**) Protein levels of TNF - α, IL-6, and IL-10. Data are expressed as mean ± SEM ($n = 6$). $^{**}p < 0.01$, $^{***}p < 0.001$ vs. Control; $^{\#}p < 0.05$, $^{\#\#}p < 0.01$, $^{\#\#\#}p < 0.001$ vs. NaF (one-way ANOVA, GraphPad Prism 8).

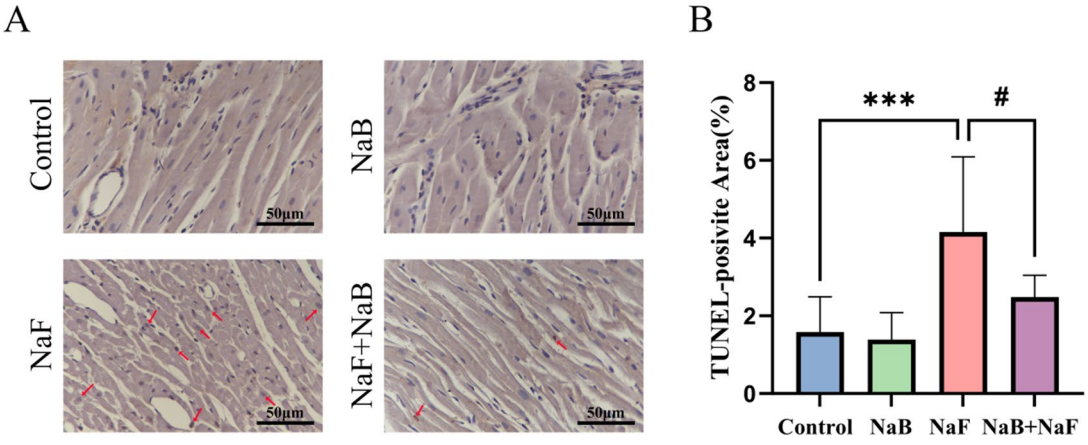

Fig. 4. TUNEL (Terminal Deoxynucleotidyl Transferase-Mediated dUTP Nick-End Labeling) analysis of cardiac apoptosis. (**A**) Quantify TUNEL positive regions in different groups of rat heart tissue samples ($n = 9$ samples). Representative images (Brown particle precipitation of cell nuclei: TUNEL+; indicated by red arrows). Scale bar: 50 μm (40× objective lens). Quantification of TUNEL-positive area proportion (apoptotic index) from 3 random fields per rat (3 rats per group, 9 total fields per group). (**B**) Statistical analysis of apoptosis rate of cardiac cells in 4 groups of rats. $^{***}p < 0.001$ vs. Control; $^{\#}p < 0.05$ vs. NaF (one-way ANOVA, GraphPad Prism 8).

Notably, NaB exerts systemic protection—mitigating fluoride-induced hepatotoxicity[25], neurotoxicity[27], and renal inflammation—suggesting conserved regulatory effects on redox and inflammation, which strengthens its translational value for multi-organ fluorosis damage.

This study provides the first evidence that NaB mitigates NaF-induced cardiac injury in rats. The heart-to-brain weight ratio (a sensitive systemic toxicity indicator) confirmed cardiac targeting: NaF reduced heart weight (0.85 ± 0.04 g vs. Control 1.09 ± 0.05 g, $p < 0.01$) and the ratio (0.45 ± 0.02 vs. Control 0.55 ± 0.01, $p < 0.01$), while

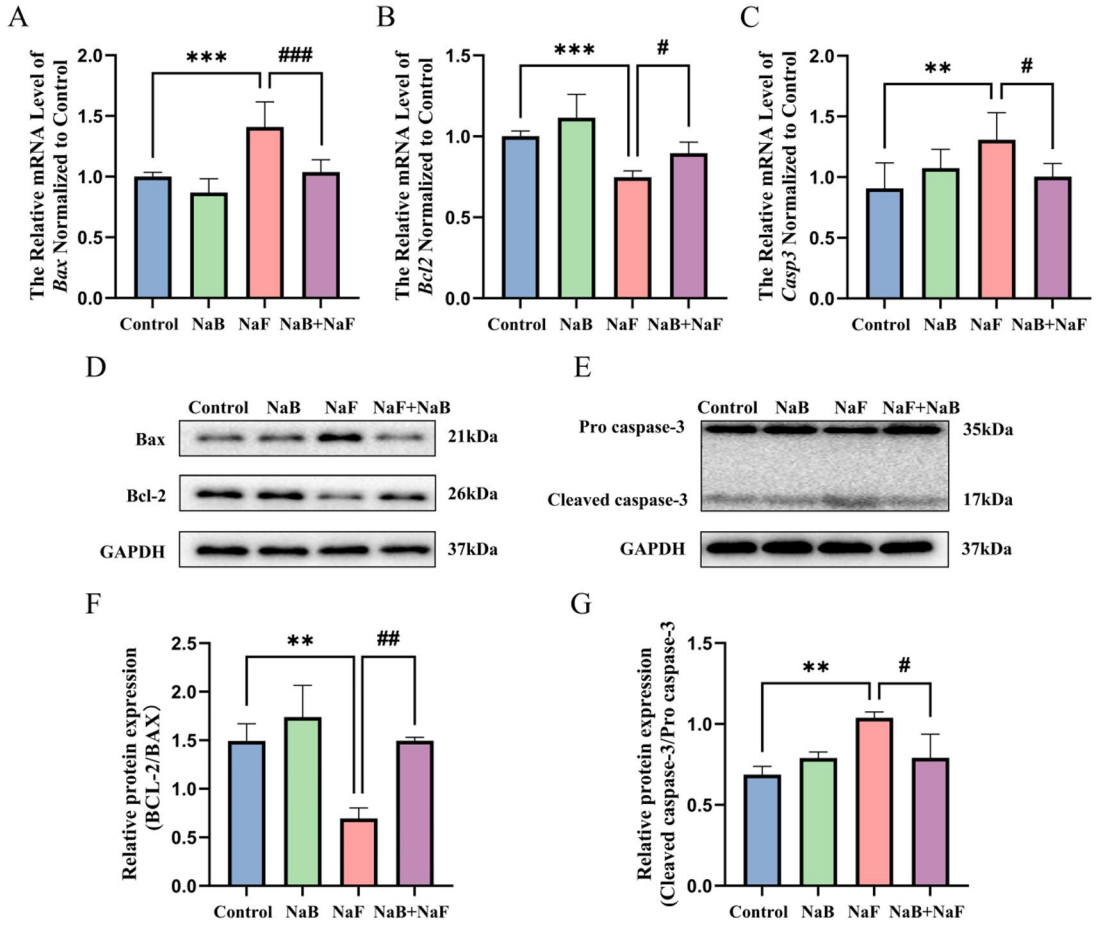

Fig. 5. NaF and NaB effects on apoptosis regulators. (**A**–**C**) mRNA levels of apoptosis regulators (*Bax*, *Bcl2*, *Casp3*). Data are expressed as mean ± SEM ($n = 6$); (**D**–**G**) Protein levels (Western blot) of Bcl-2/Bax (anti-apoptotic/pro-apoptotic ratio) and cleaved Caspase-3/pro-Caspase-3 (caspase activation marker). Data are expressed as mean ± SEM ($n = 3$). $^{**}p < 0.01$, $^{***}p < 0.001$ vs. Control; $^{\#}p < 0.05$, $^{\#\#}p < 0.01$, $^{\#\#\#}p < 0.001$ vs. NaF (one-way ANOVA, GraphPad Prism 8).

NaB restored the ratio (0.54 ± 0.03, $p < 0.05$ vs. NaF) by normalizing heart weight—highlighting targeted cardio protection.

We identified a primary pattern of atrophy and apoptotic in cardiac tissue. NaF exposure significantly depleted cTnI (25.94 ± 0.67 ng/g vs. Control 32.15 ± 1.27 ng/g, $p < 0.001$), indicative of compromised myocardial integrity. Concurrently, LDH levels were lower (89.18 ± 2.35 ng/g vs. Control 112.2 ± 4.63 ng/g, $p < 0.001$), potentially reflecting a reduction in viable tissue mass distinct from typical necrotic damage[34].This injury phenotype was synchronized with oxidative stress (↑MDA), inflammation (↑TNF-α/↓IL-10), and apoptosis (↓Bcl-2/Bax, ↑caspase-3, TUNEL^{+} cells). NaB administration reversed these changes, affirming its core protective role through antioxidant, anti-inflammatory, and anti-apoptotic effects.

Oxidative stress is central to NaF cardiotoxicity (↑MDA, ↓SOD/CAT)[35–37]. NaB likely alleviates this via Nrf2/HO-1 activation[38], though upstream signaling was unquantified. For inflammation, NaB (as an HDACi) exerts epigenetic control: it inhibits HDACs to enhance anti-inflammatory IL-10 transcription and stabilize IκBα (blocking NF-κB translocation)[18,19,39–41]. For apoptosis, it upregulates Bcl2 via promoter acetylation and inactivates p53—directly reversing pathway imbalances. This is consistent with the viewpoint of Xing et al.[42], and may involve upstream regulation of kinases (e.g., PI3K/Akt)[43]. Our data confirm NaB alleviates apoptosis indirectly: it first restores redox balance (↓MDA, ↑SOD/CAT, Fig. 2), then normalizes inflammation (↓TNF-α/IL-6, ↑IL-10, Fig. 3), thereby blocking downstream apoptotic activation. This sequence matches fluoride's "ROS→ inflammation→ apoptosis" toxic cascade. Butyrate's anti-apoptotic role in preserving mitochondrial integrity further supports our findings[44,45].

Chronic NaB may also modulate systemic inflammation via gut microbiota: it fosters beneficial taxa[46,47], reverses fluoride-induced dysbiosis[21], and strengthens the gut barrier—reducing circulating pro-inflammatory cytokines and forming a "gut-heart axis" loop[28], aligning with its systemic regulatory role. Notably, NaB's reduction of serum and urinary fluoride levels may be attributed to its regulation of physiological barriers: it strengthens the intestinal barrier to reduce fluoride absorption and protects renal tubules to promote fluoride excretion, which aligns with its known role in maintaining gut and renal integrity[24,48].

Collectively, this study confirms that chronic fluorosis induces cardiac injury through oxidative stress, inflammation, and apoptosis, and demonstrates that sodium butyrate (NaB) significantly counteracts these effects. The protective mechanisms may be involve NRF2-mediated antioxidant enhancement alongside suppression of ROS[49,50], as well as inhibition of NF-κB nuclear translocation and pro-inflammatory cytokines via epigenetic regulation, exerting the therapeutic effects of sodium butyrate on antioxidant, anti-inflammatory, and anti-apoptotic properties[48,51].

Despite focusing on the oxidative stress-inflammation-apoptosis axis, our findings hold important translational value for addressing endemic soft tissue fluorosis. Sodium butyrate is low-cost and low-toxicity, making it a practical option for resource-limited fluorosis-endemic areas where populations face long-term fluoride exposure. Moreover, the oxidative stress-inflammation-apoptosis axis targeted in this study is also involved in fluoride-induced damage to other soft tissues (e.g., liver and brain)[25,27], suggesting that NaB may have potential as a multi-organ protective agent for soft tissue fluorosis.

However, this study has limitations. Mechanistically, we focused on verifying the regulatory role of NaB in the 'oxidative stress-inflammation-apoptosis axis' but did not directly evaluate upstream signaling pathways that mediate these effects. (e.g., Nrf2 nuclear translocation, NF-κB p65 phosphorylation)[38,41]. Experimentally, single NaB/NaF doses preclude dose-response analysis[24]; exclusive male rats limit generalization (hormonal differences affect fluoride susceptibility[33]; and absent echocardiography hinders linking structure to function[5]. We also did not assess gut microbiota/metabolites[21,47]. Additionally, although the 1000 mg/kg dose of NaB used in rats translates—based on body surface area normalization—to a human-equivalent dose of approximately 2100 mg/day for a 70-kg adult, which falls within the well-tolerated range (1500–3000 mg/day) reported in human studies, clinical trials remain necessary to confirm its efficacy[46].

Future research will target upstream signaling, incorporate dose-response designs, both sexes/species, functional assays, and microbiota profiling—enhancing scientific depth and translation.

Conclusion

In summary, this study demonstrates that NaB confers significant protection against NaF-induced cardiac injury in rats, primarily through modulating oxidative stress, inflammation, and apoptosis pathways. These findings position NaB as a promising therapeutic agent for fluoride-induced cardiotoxicity.

Data availability

The datasets used and/or analysed during the current study are available from the corresponding author on reasonable request.

Received: 18 July 2025; Accepted: 29 November 2025
Published online: 02 December 2025

References

1. Solanki, Y. S., Agarwal, M., Gupta, A. B., Gupta, S. & Shukla, P. Fluoride occurrences, health problems, detection, and remediation methods for drinking water: A comprehensive review. *Sci. Total Environ.* **807**(Pt 1), 150601 (2022).
2. Kumar, P. et al. A review on fluoride contamination in groundwater and human health implications and its remediation: A sustainable approaches. *Environ. Toxicol. Pharmacol.* **106**, 104356 (2024).
3. Do, L. G. et al. Early childhood exposures to fluorides and cognitive neurodevelopment: A population-based longitudinal study. *J. Dent. Res.* **104**(3), 243–250 (2025).
4. Taylor, K. W. et al. Fluoride exposure and children's IQ scores: A systematic review and meta-analysis. *JAMA Pediatr.* **179**(3), 282–292 (2025).
5. Ullah, R., Zafar, M. S. & Shahani, N. Potential fluoride toxicity from oral medicaments: A review. *Iran. J. Basic. Med. Sci.* **20**(8), 841–848 (2017).
6. Liu, H. et al. Assessment of relationship on excess fluoride intake from drinking water and carotid atherosclerosis development in adults in fluoride endemic areas, China. *Int. J. Hyg. Environ. Health*. **217**(2-3), 413–420 (2014).
7. Maheshwari, N., Qasim, N., Anjum, R. & Mahmood, R. Fluoride enhances generation of reactive oxygen and nitrogen species, oxidizes hemoglobin, lowers antioxidant power and inhibits transmembrane electron transport in isolated human red blood cells. *Ecotoxicol. Environ. Saf.* **208**, 111611 (2021).
8. Pérez-Galicia, A. et al. Left ventricular mass and systolic function in children environmentally exposed to fluoride. *Environ. Res.* **281**, 121932 (2025).
9. Quadri, J. A. et al. Fluoride induced tissue hypercalcemia, IL-17 mediated inflammation and apoptosis lead to cardiomyopathy: ultrastructural and biochemical findings. *Toxicology* **406–407**, 44–57 (2018).
10. Yang, S. et al. Sodium fluoride induces apoptosis and alters bcl-2 family protein expression in MC3T3-E1 osteoblastic cells. *Biochem. Biophys. Res. Commun.* **410**(4), 910–915 (2011).
11. Ijomone, O. M. et al. Sex-dependent metal accumulation and immunoexpression of Hsp70 and Nrf2 in rats' brain following manganese exposure. *Environ. Toxicol.* **37**(9), 2167–2177 (2022).
12. Juan, C. A., de la Pérez, J. M., Plou, F. J. & Pérez-Lebeña, E. The chemistry of reactive oxygen species (ROS) revisited: outlining their role in biological macromolecules (DNA, lipids and proteins) and induced pathologies. *Int. J. Mol. Sci.* **22**(9) (2021).
13. Zheng, J. et al. Fluoride induces immune-inflammatory disorder in the kidneys via histone lysine crotonylation in vivo. *Ecotoxicol. Environ. Saf.* **288**, 117385 (2024).
14. Yan, X. et al. Sodium fluoride induces apoptosis in H9c2 cardiomyocytes by altering mitochondrial membrane potential and intracellular ROS level. *Biol. Trace Elem. Res.* **166**(2), 210–215 (2015).
15. Cai, K. et al. Programmed death of cardiomyocytes in cardiovascular disease and new therapeutic approaches. *Pharmacol. Res.* **206**, 107281 (2024).
16. Zhang, C. et al. Novel mechanism of fluoride induced cardiovascular system injury by regulating p53/miR200c-3p during endothelial dysfunction. *Environ. Res.* **271**, 121102 (2025).
17. Sotili, M. R. et al. Fluoride: a double-edged sword in public health and environmental toxicology. *Environ. Monit. Assess.* **197**(7), 710 (2025).
18. Yan, X. et al. Comparative transcriptomics reveals the role of the toll-like receptor signaling pathway in fluoride-induced cardiotoxicity. *J. Agric. Food Chem.* **67**(17), 5033–5042 (2019).

19. Zhang, L. et al. Hypothermia regulates mitophagy and apoptosis via PINK1/Parkin-VDAC 3 signaling pathway during oxygen-glucose deprivation/recovery injury. *Sci. Rep.* **15**(1), 4607 (2025).
20. Bian, Z. et al. Sodium butyrate inhibits oxidative stress and NF-κB/NLRP3 activation in dextran sulfate sodium salt-induced colitis in mice with involvement of the Nrf2 signaling pathway and mitophagy. *Dig. Dis. Sci.* **68**(7), 2981–2996 (2023).
21. Zhang, L. et al. Butyrate alleviates alcoholic liver disease-associated inflammation through macrophage regulation and polarization via the HDAC1/miR-155 axis. *Int. Immunopharmacol.* **131**, 111852 (2024).
22. Kang, X. et al. Roseburia intestinalis generated butyrate boosts anti-PD-1 efficacy in colorectal cancer by activating cytotoxic CD8(+) T cells. *Gut* **72**(11), 2112–2122 (2023).
23. Sun, S. et al. Sodium butyrate protects against high-fat diet-induced oxidative stress in rat liver by promoting expression of nuclear factor E2-related factor 2. *Br. J. Nutr.* **122**(4), 400–410 (2019).
24. Li, W. et al. The hepatoprotective effect of sodium butyrate on hepatic inflammatory injury mediated by the NLRP3 inflammatory pathway in subchronic fluoride-exposed mice. *Mol. Biol. Rep.* **51**(1), 1022 (2024).
25. Xia, J. et al. Sodium butyrate attenuates oxidative stress, apoptosis, and excessive mitophagy in sodium fluoride-induced hepatotoxicity in rats. *Ecotoxicol. Environ. Saf.* **291**, 117821 (2025).
26. Li, Y. et al. Sodium butyrate alleviates lead-induced neuroinflammation and improves cognitive and memory impairment through the ACSS2/H3K9ac/BDNF pathway. *Environ. Int.* **184**, 108479 (2024).
27. Li, Y. et al. Sodium butyrate ameliorates fluorosis-induced neurotoxicity by regulating hippocampal glycolysis in vivo. *Biol. Trace Elem. Res.* **201**(11), 5230–5241 (2023).
28. Yu, Z. et al. Oral supplementation with butyrate improves myocardial ischemia/reperfusion injury via a gut-brain neural circuit. *Front. Cardiovasc. Med.* **8**, 718674 (2021).
29. Jha, S. K. et al. Fluoride in groundwater: toxicological exposure and remedies. *J. Toxicol. Environ. Health B Crit. Rev.* **16**(1), 52–66 (2013).
30. Shaji, E. Fluoride contamination in groundwater: A global review of the status, processes, challenges, and remedial measures. *Geosci. Front.* **15**(2), 101734 (2024).
31. Wei, W., Pang, S. & Sun, D. The pathogenesis of endemic fluorosis: research progress in the last 5 years. *J. Cell. Mol. Med.* **23**(4), 2333–2342 (2019).
32. Zhu, X. et al. Integrative transcriptome and metabolome analysis of fluoride exposure induced developmental neurotoxicity in mouse brain. *Ecotoxicol. Environ. Saf.* **269**, 115752 (2024).
33. Oyagbemi, A. A. et al. Cardioprotective and renoprotective effects of melatonin and vitamin E on fluoride-induced hypertension and renal dysfunction in rats. *Comp. Clin. Pathol.* **33**(1), 33–45 (2024).
34. Fasakin, O. W., Awosika, A., Ogunsanya, S. T., Benson, I. O. & Olopoda, A. I. Anti-hypertensive effect of enriched white melon seed protein concentrate biscuit on sodium fluoride exposed rats. *World J. Exp. Med.* **15**(2), 105798 (2025).
35. Sharma, P., Verma, P. K., Sood, S., Singh, M. & Verma, D. Impact of chronic sodium fluoride toxicity on antioxidant capacity, biochemical parameters, and histomorphology in cardiac, hepatic, and renal tissues of wistar rats. *Biol. Trace Elem. Res.* **201**(1), 229–241 (2023).
36. Wang, D. et al. Novel pathways of fluoride-induced hepatotoxicity: P53-dependent ferroptosis induced by the SIRT1/FOXOs pathway and Nrf2/HO-1 pathway. *Comp. Biochem. Physiol. C Toxicol. Pharmacol.* **264**, 109526 (2023).
37. Li, M. et al. Fluoride exposure confers NRF2 activation in hepatocyte through both canonical and non-canonical signaling pathways. *Environ. Toxicol.* **39**(1), 252–263 (2024).
38. Hua, X. et al. Sodium butyrate alleviates experimental autoimmune prostatitis by inhibiting oxidative stress and NLRP3 inflammasome activation via the Nrf2/HO-1 pathway. *Prostate* **84**(7), 666–681 (2024).
39. Sun, J. et al. Sodium butyrate attenuates microglia-mediated neuroinflammation by modulating the TLR4/MyD88/NF-κB pathway and microbiome-gut-brain axis in cardiac arrest mice. *Mol. Brain.* **18**(1), 13 (2025).
40. Liu, H. et al. Butyrate: A double-edged sword for health? *Adv. Nutr.* **9**(1), 21–29 (2018).
41. Daniel, P. T., Schulze-Osthoff, K., Belka, C. & Güner, D. Guardians of cell death: the Bcl-2 family proteins. *Essays Biochem.* **39**, 73–88 (2003).
42. Xing, J. J. et al. Maltol mitigates cisplatin-evoked cardiotoxicity via inhibiting the PI3K/Akt signaling pathway in rodents in vivo and in vitro. *Phytother Res.* **36**(4), 1724–1735 (2022).
43. Mathew, O. P. et al. Cellular effects of butyrate on vascular smooth muscle cells are mediated through disparate actions on dual targets, histone deacetylase (HDAC) activity and PI3K/Akt signaling network. *Int. J. Mol. Sci.* **20**(12) (2019).
44. Weiss, S. L., Zhang, D., Farooqi, S. & Wallace, D. C. Sodium butyrate reverses lipopolysaccharide-induced mitochondrial dysfunction in lymphoblasts. *J. Cell. Mol. Med.* **26**(11), 3290–3293 (2022).
45. Pedersen, S. S. et al. The gut microbial metabolite butyrate alleviates IL-1β-Induced mitochondrial dysfunction and oxidative stress in pancreatic Islets. *Faseb j.* **39**(11), e70623 (2025).
46. Kalkan, A. E. et al. Beyond the gut: unveiling butyrate's global health impact through gut health and dysbiosis-related conditions: A narrative review. *Nutrients*. **17**(8) (2025).
47. Guan, X., Sun, C., Su, J., Sun, Z. & Cheng, C. Deciphering the causality of gut microbiota, circulating metabolites and heart failure: a mediation Mendelian. *Front. Pharmacol.* **16**, 1531384 (2025).
48. Peng, K. et al. Butyrate inhibits the HDAC8/NF-κB pathway to enhance Slc26a3 expression and improve the intestinal epithelial barrier to relieve colitis. *J. Agric. Food Chem.* **72**(44), 24400–24416 (2024).
49. Tang, X. et al. Sodium butyrate protects against oxidative stress in high-fat-diet-induced obese rats by promoting GSK-3β/Nrf2 signaling pathway and mitochondrial function. *J. Food Biochem.* **46**(10), e14334 (2022).
50. Song, C. et al. AMPK/p38/Nrf2 activation as a protective feedback to restrain oxidative stress and inflammation in microglia stimulated with sodium fluoride. *Chemosphere* **244**, 125495 (2020).
51. Liu, T. et al. Short-chain fatty acids suppress lipopolysaccharide-induced production of nitric oxide and proinflammatory cytokines through Inhibition of NF-κB pathway in RAW264.7 cells. *Inflammation* **35**(5), 1676–1684 (2012).

Acknowledgements

We thank all members of the Department of Human Anatomy, School of Basic Medicine, Shenyang Medical College, and the Liaoning Province Key Laboratory for Phenomics of Human Ethnic Specificity and Critical Illness for their technical support and valuable discussions during the study. We also appreciate the contributions of the experimental animals care team for maintaining the animal models.

Author contributions

Qin Mengru, Li Qianyu, Zhang Zhe, and Liu Shuyu participated in Investigation; among them, Li Qianyu, Zhang Zhe, Zhao Yubo, Liu Shuyu, and Sun Zhenxiang were responsible for Data curation. Zhao Yubo was involved in Software. Sun Zhenxiang contributed to Methodology. Duan Xiaoxu, Li Xin, Shao Bing, and Wang Zhengdong provided Supervision; Duan Xiaoxu, Ren Fu, and Wang Zhengdong participated in Conceptualization. Li Xin, Shao Bing, Yan Nan, Ren Fu, and Wang Zhengdong were in charge of Funding acquisition. Yan Nan conducted

Validation and Writing – review & editing. Ren Fu provided Resources. Meng Lu was responsible for Writing – original draft, Visualization, Investigation, and Data curation.

Funding
This study was supported by the National Natural Science Foundation of China (NSFC, No. 81803200); the Team Construction Project of Liaoning Province Education Department (No. LJ222410164002); the Basic Research Project of Liaoning Provincial Department of Education (JYTMS20231391); the Liaoning Provincial Department of Education (No. LJ222410164024, No. LJ222410164030); the Liaoning Province Science and Technology Joint Plan (Technology Research and Development Program Project, No. 2024JH2/102600237); the Shenyang Medical College Horizontal Research Project (No. SYKT2025002, No. SYKT2025005, No. SYKT2025007); the Shenyang Science and Technology Plan Project (22-321-33-99); the Science Project of Central Hospital of Shenyang Sujiatun (Grant No. 320100002001); and the Team Construction Project of Liaoning Province Education Department (LJ222410164013).

Declarations

Competing interests
The authors declare no competing interests.

Additional information
Supplementary Information The online version contains supplementary material available at https://doi.org/10.1038/s41598-025-31105-y.

Correspondence and requests for materials should be addressed to F.R. or Z.W.